https://doi.org/10.5194/egusphere-2025-722
Preprint. Discussion started: 15 April 2025

SERGHEI v2.1: a Lagrangian Model for Passive Particle Transport using a 2D Shallow Water Model (SERGHEI-LPT)

Pablo Vallés[a,b], Mario Morales-Hernández[a], Volker Roeber[b], Pilar García-Navarro[a], and Daniel Caviedes-Voullième[c,c2]

[a]I3A, University of Zaragoza, Zaragoza (Spain)
[b]E2S Chair HPC-Waves, University of Pau, Anglet (France)
[c]Institute of Bio- and Geosciences: Agrosphere (IBG-3), Forschungszentrum Jülich, Jülich (Germany)
[c2]Simulation and Data Lab. Terrestrial Systems, Jülich Supercomputing Centre (JSC), Forschungszentrum Jülich, Jülich (Germany)

Correspondence: Daniel Caviedes-Voullième (d.caviedes.voullieme@fz-juelich.de)

Abstract. This paper presents a Lagrangian model for particle transport driven by a 2D shallow water model, assuming that the particles have negligible mass and volume, are located at the free surface, and without interactions between them. Particle motion is based on advection and turbulent diffusion, which is added using a random-walk model. The equations for particle advective transport are solved using the flow velocity provided by a 2D shallow water solver and an online first-order Euler method, an online fourth order Runge-Kutta method and an offline fourth order Runge-Kutta method. The primary objective of this work is to analyze the accuracy and computational efficiency of the numerical schemes and the algorithm implementation for particle transport. To verify the accuracy and computational cost, several test cases inspired by laboratory setups are simulated. In this analysis, the Euler online method provides the best compromise between accuracy and computational efficiency. Finally, a localized precipitation event in the Arnás catchment is simulated to test the model's capability to represent particle transport in overland flow over irregular topography.

1 Introduction

Over the past decade, floods have emerged as the most destructive natural disaster worldwide (Wallemacq et al., 2015; for Research on the Epidemiology of Disasters , CRED), resulting in substantial and progressively increasing economic losses (Formetta and Feyen, 2019; Ripple et al., 2020). Projections suggest that in the coming decades, both economic losses and the number of individuals affected by floods are expected to rise (Dottori et al., 2018; OECD, 2016). This situation forces institutions to develop strategies and tools to predict and mitigate the damage caused by floods. Potential solutions range from administrative policies based on practical actions (Nations, 2015; Olcina et al., 2016; Martin et al., 2010) to the development of computational prediction tools (Bates et al., 2023; Thielen et al., 2009; Chen et al., 2009). In recent years, these predictive tools, which rely on numerical simulations, have seen significant advancements in both accuracy and computational efficiency (Sampson et al., 2015; Knijff et al., 2010; Lacasta et al., 2014). Some models are based on the two-dimensional Shallow Water Equations (SWE), offering accurate results with high computational efficiency (Xia et al., 2019; Morales-Hernández et al.,

https://doi.org/10.5194/egusphere-2025-722
Preprint. Discussion started: 15 April 2025

2021). However, the majority of models used for flood forecasting in rivers do not account for the transport of objects, such as vehicles, waste containers and other urban flood drifters (Bayón et al., 2024), or wood, carried by the flow during flooding events. This omission reduces the completeness of these tools, as object transport is a critical component of floods and can cause obstructions in hydraulic structures within channels and streams, thereby exacerbating the damage during such events (Bayón et al., 2024; Valero et al., 2024; Lofty et al., 2024). Several studies have examined debris accumulation near weirs, culverts, and dams, highlighting their significant impact on flood risk (Thomas and Nisbet, 2012; De Cicco et al., 2015). Moreover, the transport of objects by geophysical flows is related to other issues, such as environmental accidents due to pollutant spills in rivers and lakes (van Emmerik et al., 2022; Ivshina et al., 2015; Mellink et al., 2024), and environmental impact studies concerning seed dispersion by precipitation in catchments (Zamora and Montagnini, 2007; Sánchez-Salas et al., 2017), among others.

The transport of objects by fluid flows has been extensively studied in recent years (Braudrick and Grant, 2000; Xia et al., 2011; Martínez-Gomariz et al., 2020). These studies have led to the development of computational models for simulating the transport of particles with negligible mass or volume (Finaud-Guyot et al., 2023), as well as contaminants and small objects such as microplastics (García-Martínez and Flores-Tovar, 1999; Jalón-Rojas et al., 2019), sediments, bedload transport (Zhao et al., 2024; Baharvand et al., 2023), and macroscopic objects (Persi et al., 2018a, b). Debris transport can be analyzed using either an Eulerian or a Lagrangian framework (Nordam et al., 2023). The Lagrangian approach offers detailed insights into individual processes affecting debris, such as deposition, fragmentation, and degradation, and is particularly useful when the number of debris particles is relatively low. On the other hand, the Eulerian approach provides a different approach by treating debris as a concentration, offering greater computational efficiency than the Lagrangian method when the number of bodies is really high. However, the Eulerian description is inherently dispersive and does not account for the specific transport trajectories of particles, thereby overlooking certain small-scale details (Cai et al., 2023).

In recent decades, numerous computational models have been developed to simulate particle transport. However, the majority of these models are designed for coastal scenarios where challenging wet-dry transitions do not occur (García-Martínez and Flores-Tovar, 1999; Lebreton et al., 2012; Liubartseva et al., 2018). Furthermore, some models update particle positions only at specific time intervals rather than at every time step, in order to reduce the high computational cost (Finaud-Guyot et al., 2023). The main reason for using this kind of methods, commonly known as offline methods, is due to the non-presence of dry-wet problem when they are used in marine environments. Thus, the inaccuracy of updating every certain period of time is compensated by using higher-order models, such as a fourth-order Runge-Kutta method (García-Martínez and Flores-Tovar, 1999). An alternative approach is to determine the temporal evolution of material by solving the Eulerian advection-dispersion equation, thereby obtaining the changes in debris concentration over time (Baharvand et al., 2023; Schreyers et al., 2024; Portillo De Arbeloa and Marzadri, 2024). While these models effectively capture the behavior of large quantities of small debris, they are not suitable for large objects or scenarios involving a small number of material particles. Furthermore, some Lagrangian models are implemented using three-dimensional hydrodynamic frameworks (Jalón-Rojas et al., 2019; Pilechi et al., 2022), which provide more detailed flow information compared to two-dimensional and one-dimensional models, albeit at the cost of increased computational time.

https://doi.org/10.5194/egusphere-2025-722
Preprint. Discussion started: 15 April 2025

In addition to advection, turbulent diffusion can play an important role in the material transport, not only in water (Merritt and Wohl, 2002; Molazadeh et al., 2024; Yang and Foroutan, 2023), but also in other environments such as wind (Horn et al., 2012). Thus, it is interesting to add to the Lagrangian model of material transport some kind of minimal turbulence model to achieve greater realism and accuracy in the numerical results (Jalón-Rojas et al., 2019; Liubartseva et al., 2018).

Finally, in order to be effective, the computational model must be both accurate and computationally efficient. The balance between computational efficiency and accuracy is crucial, particularly for operational prediction tools, where timely and reliable results are essential. In this context, two-dimensional hydrodynamic models offer a high degree of accuracy with lower computational costs compared to three-dimensional models (Vacondio et al., 2016; Echeverribar et al., 2019).

This work represents an initial step towards a Lagrangian model for material transport in shallow water flows. The material simulated in this study are particles with negligible mass and volume that do not interact with each other, thus representing a simplified case. The primary objective is to analyze the accuracy and computational efficiency of the numerical scheme and the algorithm implementation for particle transport. The accuracy and efficiency of an explicit Euler method are compared with those of a fourth order Runge-Kutta method. Additionally, these methods are evaluated both when applied at every time step or iteration, and at specific iteration intervals. Furthermore, particles dispersion is incorporated into the Lagrangian model equations using a random-walk model because the hydrodynamic model does not resolve turbulence. All analyzes are based on simulations of both analytical and laboratory test cases and realistic scenarios. The model is driven by an Eulerian hydrodynamic framework based on the SWE to describe flow evolution. The implementation of these techniques is part of an ongoing initiative to create a modeling framework grounded in physically-based hydrodynamics: the SERGHEI (Simulation Environment for Geomorphology, Hydrodynamics, and Ecohydrology in Integrated form) model (Caviedes-Voullième et al., 2023). The code developed for this study is open-source and available at https://gitlab.com/serghei-model.

The structure of the paper is as follows: first, the governing equations for the hydrodynamic model and for the Lagrangian model are presented; second, the numerical schemes and their details are presented; then, analytical, test and realistic cases are simulated; and finally, the conclusions of the present work are shown.

2 Governing equations

The equations flow are presented and subsequently, the equations corresponding to passive particle transport are discussed.

2.1 2D Shallow Water Equations

The hydrodynamic model characterizes surface flow through the hyperbolic 2D SWE system, which is based on the mass and momentum conservation (Cunge et al., 1989):

$$\frac{\partial h}{\partial t} + \nabla(h\mathbf{u}) = r - i + e + S_w \tag{1}$$

https://doi.org/10.5194/egusphere-2025-722
Preprint. Discussion started: 15 April 2025

$$\frac{\partial hu}{\partial t} + \frac{\partial}{\partial x}\left(u^2 + \frac{1}{2}gh^2\right) + \frac{\partial (huv)}{\partial y} = -ghS_{fx} - gh\frac{\partial z_b}{\partial x} \tag{2}$$

$$\frac{\partial hv}{\partial t} + \frac{\partial}{\partial y}\left(v^2 + \frac{1}{2}gh^2\right) + \frac{\partial (huv)}{\partial x} = -ghS_{fy} - gh\frac{\partial z_b}{\partial y} \tag{3}$$

where h is the water depth $[L]$, $\mathbf{u} = (u,v)$ is the velocity flow vector $[LT^{-1}]$, r is the precipitation rate $[LT^{-1}]$, i is the infiltration rate $[LT^{-1}]$, e is the evaporation rate $[LT^{-1}]$ and S_w denotes the flow rate $[LT^{-1}]$ provided by sources or sinks. The gravitational acceleration is denoted by $g\,[LT^{-2}]$, z_b is the bed elevation $[L]$, and S_{fx} and S_{fy} are the friction slope terms, defined as:

$$S_{fx} = \frac{n^2 u\sqrt{u^2+v^2}}{h^{4/3}}, \quad S_{fy} = \frac{n^2 v\sqrt{u^2+v^2}}{h^{4/3}} \tag{4}$$

being n the Manning's roughness coefficient $[TL^{-1/3}]$ (Arcement and Schneider, 1984).

2.2 Particle tracking equations

In a Lagrangian model of material transport, material elements are entrained and transported based on hydrodynamic forces, computed with appropriate coefficients or following a kinematic approach. In this study, the transported particles act as passive tracers: they have negligible volume and mass, do not interact with each other, and do not affect the flow field.

In the absence of turbulence, particle transport is driven by advection, and the particle trajectories are governed by the following system of equations that defines the position of each particle $\mathbf{x}_p = (x_p, y_p, z_p)$:

$$\begin{cases} \dfrac{dx_p}{dt} = u(\mathbf{x}_p) \\ \dfrac{dy_p}{dt} = v(\mathbf{x}_p) \\ \dfrac{dz_p}{dt} = 0 \end{cases} \tag{5}$$

As observed, the vertical position is unaffected by the flow velocity due to the depth-averaged SWE approximation, which neglects the vertical velocity component. Consequently, the particle resides at the free water surface, which is the sum of the water depth h and the bottom level z_b. This condition prevents issues when the bottom elevation is irregular. Since the hydrodynamic model is vertically averaged, an average velocity for the flow is imposed on each cell, which could cause particles located at different vertical positions to cross obstacles or walls. Moreover, the advection velocity depends on the velocity field at the position of the particle at each time.

Turbulence effects in a flow can be significant and, by modifying the velocity field, also influence particle transport (Merritt and Wohl, 2002). Therefore, if turbulence is not incorporated into the flow velocity, as it is in the hydrodynamic model of the SERGHEI framework (Caviedes-Voullième et al., 2023), it can be included in the particle velocity, as follows:

https://doi.org/10.5194/egusphere-2025-722
Preprint. Discussion started: 15 April 2025

$$\begin{cases} \dfrac{dx_p}{dt} = u(\mathbf{x}_p) + u_{\text{disp}}(\mathbf{x}_p) \\ \dfrac{dy_p}{dt} = v(\mathbf{x}_p) + v_{\text{disp}}(\mathbf{x}_p) \\ \dfrac{dz_p}{dt} = 0 \end{cases} \tag{6}$$

where $\mathbf{v}_{\text{disp}} = (u_{\text{disp}}, v_{\text{disp}}, 0)$ is the velocity induced by the dispersion, where it is considered a null dispersion velocity in the vertical coordinate because of the lack of the advection velocity in the vertical. In this study, a random-walk model is employed to simulate dispersion because of its simplicity and its great balance between computational efficiency and accuracy (Jalón-Rojas et al., 2019). This model proposes the $\mathbf{v}_{\text{disp}}$ as a function of the diffusivity coefficients K_{hx} and K_{hy} $[L^2T^{-1}]$ in the x- and y-,coordinates, respectively. In contrast to imposing constant values based on empirical results (Jalón-Rojas et al., 2019; Peeters and Hofmann, 2015) that depends on the size and shape of the object, the diffusivity coefficients K_{hx} and K_{hy} are here derived from a velocity-dependent expression, as turbulence is directly proportional to velocity. Therefore, the standard anisotropic diffusion model (Morales-Hernández et al., 2019) is utilized to determine the diffusivity variables, with the following expressions:

$$K_{hx} = \epsilon_L |u^*| h(x_p, y_p), \quad K_{hy} = \epsilon_T |u^*| h(x_p, y_p) \tag{7}$$

where ϵ_L, and ϵ_T are the longitudinal and transversal dispersion coefficients $[L^2T^{-1}]$ (Rutherford, 1994), respectively; and $|u^*|$ is the friction velocity:

$$|u^*| = n\sqrt{g\frac{v_x^2 + v_y^2}{(h(x_p, y_p))^{1/3}}} \tag{8}$$

3 Numerical schemes

The equations (1), (2) and (3) are solved using an explicit upwind finite volume scheme, which is based on the Augmented Roe Riemann solver. We do not describe this approach here, but refer the reader to the relevant literature (Echeverribar et al., 2019; Murillo and García-Navarro, 2010; Morales-Hernández et al., 2013), and the HPC implementation within SERGHEI (Caviedes-Voullième et al., 2023).

In this paper, several numerical schemes are explored to solve the particle equations systems.

3.1 Numerical scheme for the Lagrangian particles model

To obtain the temporal and spatial evolution of the particles, it is necessary to discretize the system of equations (5) when turbulence is not considered, or system (6) when it is included. In passive particle tracking, particles are considered to have negligible mass and volume, ensuring no interaction with each other or the flow, thereby maintaining unaltered flow properties such as density or viscosity. The choice of discretization method depends on the required accuracy. In this study, two methods are utilized to discretize the equations governing particle trajectories: the forward Euler method and the Runge-Kutta method.

https://doi.org/10.5194/egusphere-2025-722
Preprint. Discussion started: 15 April 2025

3.1.1 Explicit forward Euler method

The temporal evolution of particle positions is obtained by considering the particles as mathematical points denoted by $\mathbf{p}$, which are advected in space $\mathbf{x}$ following a velocity field $\mathbf{v}$. In this model, dispersion is not calculated within the hydrodynamic module, potentially leading to unrealistic particle transport if this phenomenon is not considered (Merritt and Wohl, 2002). Although the flow still has no turbulence model, the dispersive effects of turbulence are modelled on the transport of particles. These effects are added using a random-walk model, which can generate sufficient dispersion to introduce turbulent motion (Rutherford, 1994):

$$\begin{cases} x_p^{n+1} = x_p^n + \Delta t_p^n u_i^n + R_{p,x}^n \left(2\sigma^{-1} K_{hx,i}^n \, \Delta t_p^n\right)^{1/2} \\ y_p^{n+1} = y_p^n + \Delta t_p^n v_i^n + R_{p,y}^n \left(2\sigma^{-1} K_{hy,i}^n \, \Delta t_p^n\right)^{1/2} \\ \qquad\qquad z_p^{n+1} = h_i^n + z_{b,i} \end{cases} \tag{9}$$

where the Eulerian velocity field $\mathbf{v}_i^n$ is the velocity field in cell i at time step n, in which the particle p is located, i.e., contains the point $\mathbf{x_p}^n = (x_p^n,\, y_p^n,\, z_p^n)$, h_i^n is the water depth in the cell i at time step n, $z_{b,i}$ is the bottom elevation of the cell i, and Δt_p^n is the particle time step. $R_{p,x}^n$ and $R_{p,y}^n$ are random numbers, which follow a uniform distribution with mean 0 and standard deviation $\sigma = 1$. $K_{hx,i}^n$ and $K_{hy,i}^n$ are the horizontal diffusivity in $\hat{x}$ and $\hat{y}$ components, respectively, as defined by expression (7).

3.1.2 Runge-Kutta method

The primary limitation of the explicit Euler method is its first-order accuracy, which may result in significant deviations from reality unless the time step for the Lagrangian model is sufficiently small (Bennett and Clites, 1987). Therefore, a higher-order approximation is necessary to capture the spatial variation of the velocity field when a large time step is computed by the numerical scheme. For this reason, a fourth-order Runge-Kutta method is presented for the advection formulation:

$$\mathbf{x_p}^{n+1} = \mathbf{x_p}^n + \frac{\Delta t_p^n}{6}\left(\mathbf{v}\left(\mathbf{x_p}, t^n\right) + 2\mathbf{v}\left(\mathbf{x_p} + \frac{1}{2}a, t^{n+1/2}\right) + 2\mathbf{v}\left(\mathbf{x_p} + \frac{1}{2}b, t^{n+1/2}\right) + \mathbf{v}\left(\mathbf{x_p} + c, t^{n+1}\right)\right) \tag{10}$$

where:

$$a = \Delta t_p^n \, \mathbf{v}\left(\mathbf{x_p}, t^n\right), \quad b = \Delta t_p^n \, \mathbf{v}\left(\mathbf{x_p} + \frac{1}{2}a, t^{n+1/2}\right), \quad c = \Delta t_p^n \, \mathbf{v}\left(\mathbf{x_p} + \frac{1}{2}b, t^{n+1/2}\right) \tag{11}$$

This method requires the velocity at intermediate times ($t^{n+1/2}$), which is not directly calculated by the numerical scheme. Therefore, a fourth-order interpolation is used to obtain it:

$$\mathbf{v}^{n+1/2}(\mathbf{x_p}) = \frac{5}{16}\mathbf{v}^{n+1}(\mathbf{x_p}) + \frac{15}{16}\mathbf{v}^{n}(\mathbf{x_p}) - \frac{5}{16}\mathbf{v}^{n-1}(\mathbf{x_p}) + \frac{1}{16}\mathbf{v}^{n-2}(\mathbf{x_p}) \tag{12}$$

https://doi.org/10.5194/egusphere-2025-722
Preprint. Discussion started: 15 April 2025

Comparing the equations of both methods, it is evident that the higher accuracy of the Runge-Kutta method entails a higher computational cost per time step than the explicit Euler method, as the Runge-Kutta method requires the velocity vector at four different times and the calculation of additional terms to determine the trajectory evolution.

3.2 Trajectory algorithm

The transport of the particle is governed by the advection. The trajectory can be determined directly from the initial cell to the final cell (García-Martínez and Flores-Tovar, 1999; Bennett and Clites, 1987) (see red trajectory in Figure 1a), or the particle can be moved cell by cell (see green trajectory in Figure 1b). The latter approach is compulsory for addressing potential dry-wet interface issues and for preventing particles from traversing obstacles, as shown in Figure 1b.

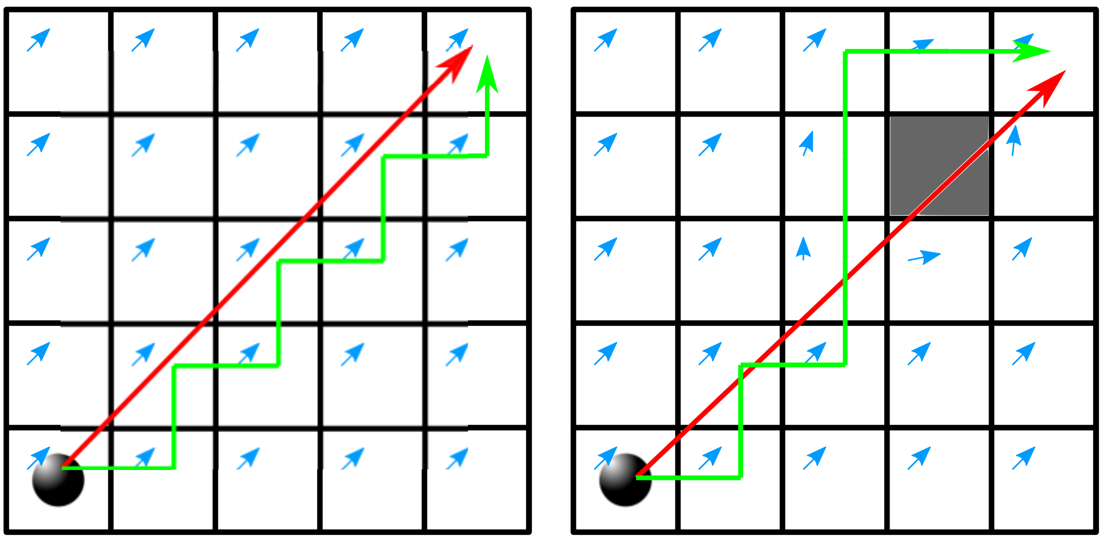

(a) (b)

Figure 1. The two possible strategies for the trajectory of particles in absence of obstacles **(a)** and the same strategies when there is an obstacle (gray cell) **(b)**.

Thus, the algorithm that loops over the particles must be carefully designed to ensure that each particle traverses each computational cell discretely, dynamically adopting the local velocity and updating its position based on the discrete flow velocities within each cell.

For that, let us consider a single particle p defined by its position $\mathbf{x_p}$ in the same position of the point $\mathbf{p} = (p_x, p_y)$, which is inside of cell i, with some velocity $\mathbf{v}_i$. Let d be the distance between the particle and the point at which the particle would leave the cell when following the velocity within the cell, as shown in Figure 2a. In this figure, $\mathbf{A}$ and $\mathbf{q}$ are the respectively lower left and right corners (respectively) of the cell, b is the distance between $\mathbf{q}$ and the intersection edge point, and $\hat{\mathbf{e}}$ is the unit vector of the Cartesian y-axis. The distance d is the minimum distance in the direction of the velocity vector $\mathbf{v}$ from the

https://doi.org/10.5194/egusphere-2025-722
Preprint. Discussion started: 15 April 2025

point $\mathbf{p}$ until it crosses an edge that separates one computational cell from the next. This distance is measured along the line defined by the unit vector $\hat{\mathbf{v}}$.

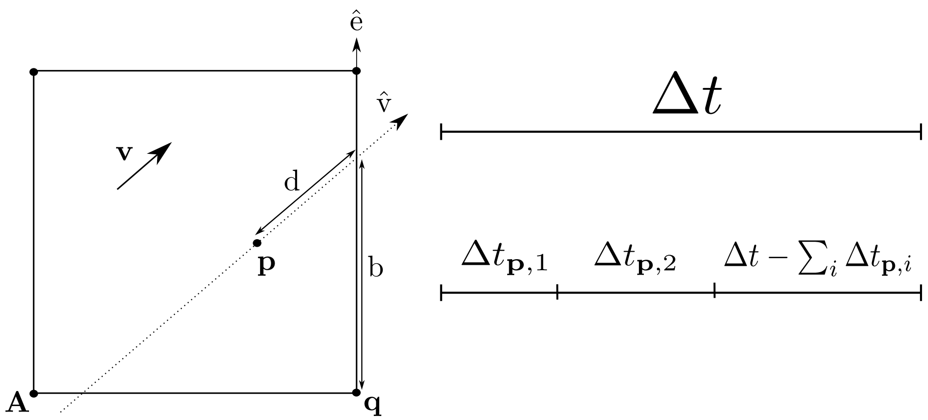

(a) (b)

Figure 2. (a) Representation of a point $\mathbf{p}$ (particle position) in a generic cell and (b) a generic representation of the time steps for 2D model and particles

In order to guarantee that the particle is not advected beyond cell i with the velocity $\mathbf{v}_i$, it is simple to see that a geometric restriction for the time step Δt_p of particle p is given by:

$$\Delta t_p \leq \frac{d}{||\mathbf{v}_i||} \tag{13}$$

This is fundamentally a CFL condition for the particle advection.

There is an additional restriction for Δt_p related to the hydrodynamic time step size Δt:

$$\Delta t_p \leq \Delta t \tag{14}$$

That is, the particle time step cannot be so large that it requires a future value of the Eulerian velocity field. However, if $\Delta t_p < \Delta t$, another condition must be introduced to ensure that particles evolve as far as the the global hydrodynamic time stepping allows. Therefore, if $\Delta t_p < \Delta t$, an iterative sub-cycling process is carried out by calculating time steps $\Delta t_{p,\,m}$ until (Figure 2b):

$$\Delta t = \sum_m \Delta t_{p,\,m} \tag{15}$$

This may produce situations as that of the Figure 3, where the particle travels through 1, 2 or (at most) 3 cells within a single 2D time step Δt.

Therefore, the restrictions for Δt_p are fully formulated as:

$$\Delta t_{p,\,m} \leq \min\left(\frac{d}{||\mathbf{v}_i||},\, \Delta t - \sum_m \Delta t_{p,\,m}\right) \tag{16}$$

https://doi.org/10.5194/egusphere-2025-722
Preprint. Discussion started: 15 April 2025

The time step restriction problem is therefore reduced to determining the distance d to the edge through which the particle will exit the cell.

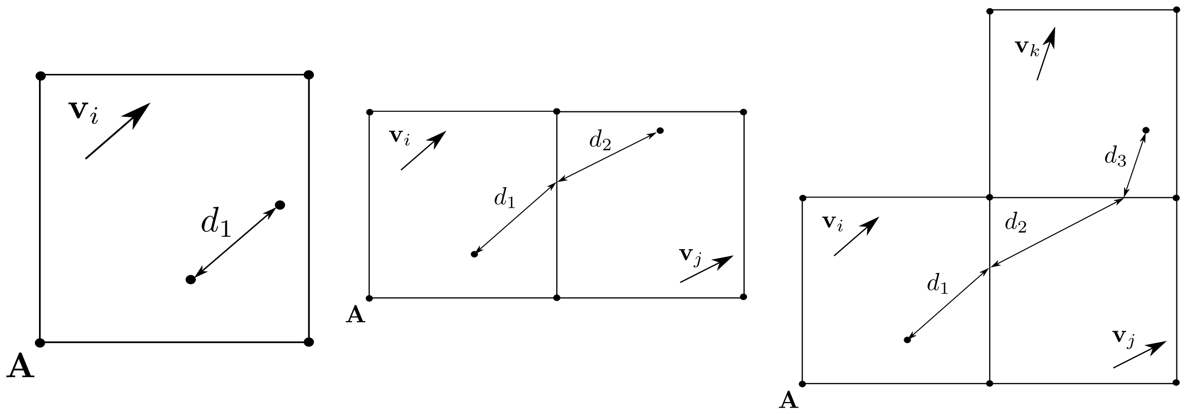

(a) (b) (c)

Figure 3. Three possible situations for a particle: traveling through 1 cell **(a)**, 2 cells **(b)**, or 3 cells **(c)** final position.

The value of d is calculated as follows:

1. Given a line with with direction $\hat{\mathbf{v}} = \mathbf{v}\,||\mathbf{v}||^{-1}$ passing through particle point $\mathbf{p}$, find its intersection with the lines defining the edges, and compute the distance d from $\mathbf{p}$ to the 4 intersection points: north, south, east and west intersections (see Figure 2):

$$\mathbf{p} + d\hat{\mathbf{v}} = \mathbf{q} + b\hat{e} \tag{17}$$

Considering only the x-coordinate:

$$p_x + d\hat{v_x} = q_x \tag{18}$$

and therefore, if $\hat{v_x}$ is not null:

$$d = \frac{q_x - p_x}{\hat{v_x}} = \frac{A_x + \Delta x - p_x}{\hat{v_x}} \tag{19}$$

where Δx is the cell length in the x-coordinate, which, being a square cell, is equivalent to the length in the y-coordinate. For cases where $\hat{v_x}$ is null or negative, the distance d calculated using (19) does not yield the correct intersection. For this reason, three additional distances d are calculated by employing a procedure analogous to that used for deriving (19):

$$d_2 = \frac{A_x - p_x}{\hat{v_x}} \qquad \text{if and only if} \quad \hat{v_x} \neq 0 \tag{20}$$

$$d_3 = \frac{A_y + \Delta x - p_y}{\hat{v_y}} \qquad \text{if and only if} \quad \hat{v_y} \neq 0 \tag{21}$$

https://doi.org/10.5194/egusphere-2025-722
Preprint. Discussion started: 15 April 2025

$$d_4 = \frac{A_y - p_y}{\hat{v_y}} \qquad \text{if and only if} \quad \hat{v_y} \neq 0 \tag{22}$$

2. Discard negative distances as these are antiparallel to the velocity vector.
3. The minimum positive distance d corresponds to the correct intersection.

Having computed d, it is possible to evaluate the particle sub-cycling time step (16), and with such time step advect the particle with (6). This algorithm is used in both the Euler and Runge-Kutta methods.

Thus, the temporal evolution of the x and y-coordinates of particles are obtained by the proposed algorithm. With respect to the z coordinate, assuming a passive particle tracking with negligible mass and volume for the particles, the value of the water surface level of the cell where the particle is located is imposed, so it is floating in it. This approach and the use of the algorithm automatically resolve issues such as: (i) the wet/dry problem, provided the numerical method accurately addresses these conditions for the flow; and (ii) wet/wet problems involving topographical changes, where a particle floating at an arbitrary vertical position within a cell may encounter an adjacent cell with a higher elevation, preventing its movement into that cell despite both cells containing water. This ensures that the particle's movement is physically feasible and adheres to the elevation constraints of the cells.

Introducing a turbulent dispersion term can cause issues in the model in wet-dry cases, as a particle could find itself in a wet cell due to advection and, by adding the dispersion term, reach a dry cell. Therefore, a restriction is added: if the cell to which the particle would travel due to the addition of the turbulence term is dry, this term is not added.

3.3 Temporal integration modes

Depending on the desired accuracy of the results, different time intervals are proposed to update the evolution of the particles. When the particle advection is computed on every time step of the hydrodynamic solver (from n to $n+1$), we say this is an online mode. However, if the new position of the particle is calculated every certain number of hydrodynamic time steps $nIter$ (from n to $n+nIter$), we consider this an offline mode. We hypothesize that the online mode provides more accurate results than the offline mode, but potentially with a higher computational cost due to a larger number of particle advection updates. Conversely, using the explicit Euler method in an offline mode is ineffective, due to its lack of accuracy; therefore, the explicit Euler scheme is only employed in the online mode. In contrast, the Runge-Kutta method is suitable for both online and offline modes.

3.4 Implementation in SERGHEI framework

The Lagrangian model for particles transport has been implemented in the SERGHEI framework, as a one of the several modules that have been implemented in this framework (see Figure 4).The SERGHEI framework is a modular and open-source simulation system designed to target performance portability across HPC (High-Performance Computing) platforms and standard workstations (Caviedes-Voullième et al., 2023). It focuses on future-proofing and sustainability while consolidating over

https://doi.org/10.5194/egusphere-2025-722
Preprint. Discussion started: 15 April 2025

a decade of mature numerical techniques for shallow water modeling. SERGHEI facilitates a modular, HPC-ready community model, enabling broader collaboration. The framework moves beyond classical fluvial flooding and hydrograph generation to address applications related to landscape function, transport, and integration into Earth System Models (ESM).

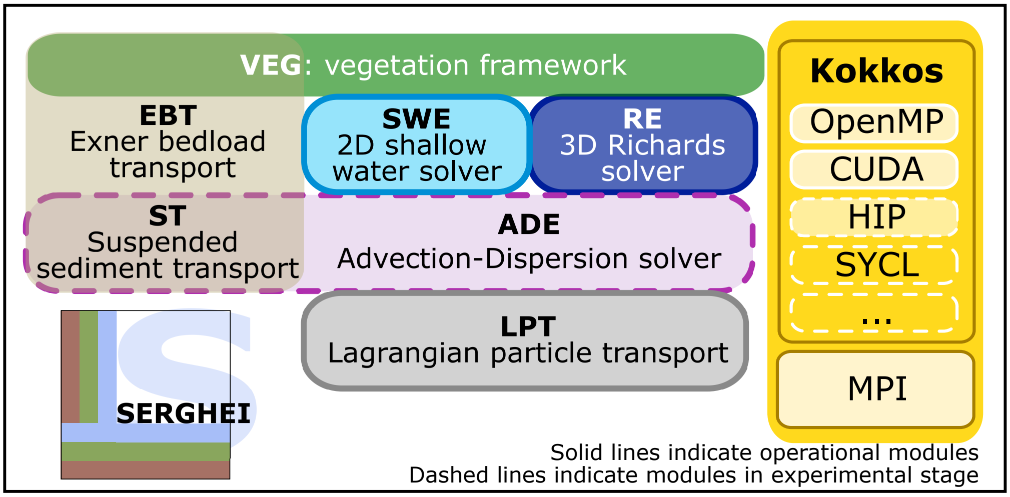

Figure 4. Conceptual diagram for the SERGHEI modules and their implementation status.

The Lagrangian model has been developed along the same lines as the other modules in SERGHEI. In this way, this model has been implemented in C++ and using the *Kokkos* performance-portability layer, which allows the simulation of the model using any GPU architecture. As can be seen in Figure 5, the Lagrangian model is updated after updating the hydrodynamic model, as it needs the updated information of the conserved variables. The implementation of the Lagrangian model for distributed computations in progress.

4 Results

The validation of the Lagrangian model is conducted through the simulation of several test cases with increasing complexity, assessing both accuracy and computational efficiency. The simulations are run using a GPU NVIDIA GeForce RTX 3060.

4.1 Steady circular vortex case

Initially, a steady circular vortex test case is simulated to validate the model's accuracy. The steady state implies that particles advected by the vortex should maintain a constant radius (Finaud-Guyot et al., 2023; García-Martínez and Flores-Tovar, 1999). The circular vortex is simulated with varying cell sizes, ensuring the particle completed four full revolutions for consistency in error measurement. The vortex radius is consistently set at $R = 100$ m, with a water depth of $h = 0.1$ m and no roughness ($n = 0$). For this test, the hydrodynamic solver is turned off, so that the Eulerian flow fields (water depth and velocity) remained constant and are not evolved over time, also resulting in a constant time step Δt throughout the simulation. Turbulent diffusion

https://doi.org/10.5194/egusphere-2025-722
Preprint. Discussion started: 15 April 2025

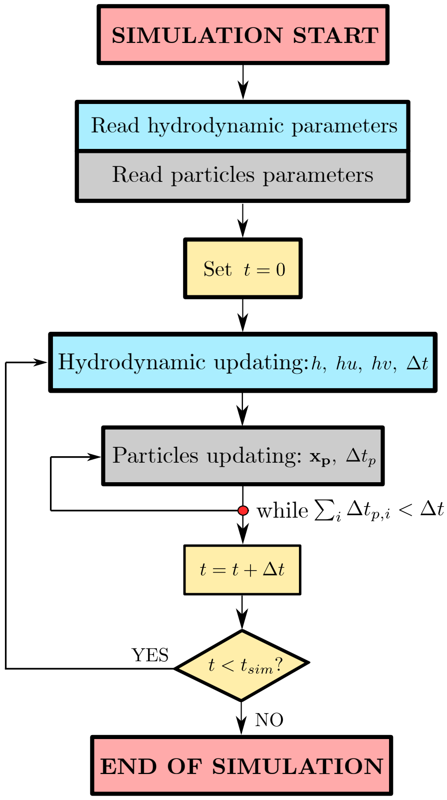

Figure 5. Schematic of the numerical calculation using the LPT module.

terms are excluded from the particle trajectory equations because this is an analytical case, and the objective is to guarantee correctness and robustness of the advection. The Runge-Kutta offline method is updated every five hydrodynamic time steps.

The errors for each grid resolution using different numerical configurations are shown in Figure 6. The L_1 norm for the error at each time step is defined by:

$$L_1(t^n) = |\mathbf{x}_\mathbf{p}^n - \hat{\mathbf{x}}| \tag{23}$$

where $\mathbf{x}_\mathbf{p}^n$ is the particle position at the time t^n and $\hat{\mathbf{x}}$ is the analytical position. The L_1 Norm integrated in time is the Mean Absolute Error (MAE), which is obtained using:

$$\mathrm{MAE} = \frac{1}{N}\sum_{n=0}^{N} L_1(t^n) \tag{24}$$

where N is the number of time measurements.

Additionally, the L_2 Norm at each time step is defined as:

$$L_2(t^n) = (\mathbf{x}_\mathbf{p}^n - \hat{\mathbf{x}})^2 \tag{25}$$

https://doi.org/10.5194/egusphere-2025-722
Preprint. Discussion started: 15 April 2025

while the Root Mean Squared Error (RMSE) is computed as:

$$\mathrm{RMSE} = \sqrt{\frac{1}{N}\sum_{n=0}^{N} L_2(t^n)} \tag{26}$$

Figure 6 shows that, under steady flow, the error of Runge-Kutta method is similar to the Euler method. The algorithm implemented provides a reduced error for the Euler method because of the calculus of the trajectory in each cell (see Figure 1) and in each time step. Moreover, the error of all methods depends strongly on the discretization of the domain, with lower errors for smaller cell sizes. Figure 6 also shows the error reduction in the same order as the Euler method as the cell size is reduced (order 1). However, for the Runge-Kutta method (order 4), the error is not observed to reduce with that order. This is mainly because it is a stationary case and the value of the time step is fixed.

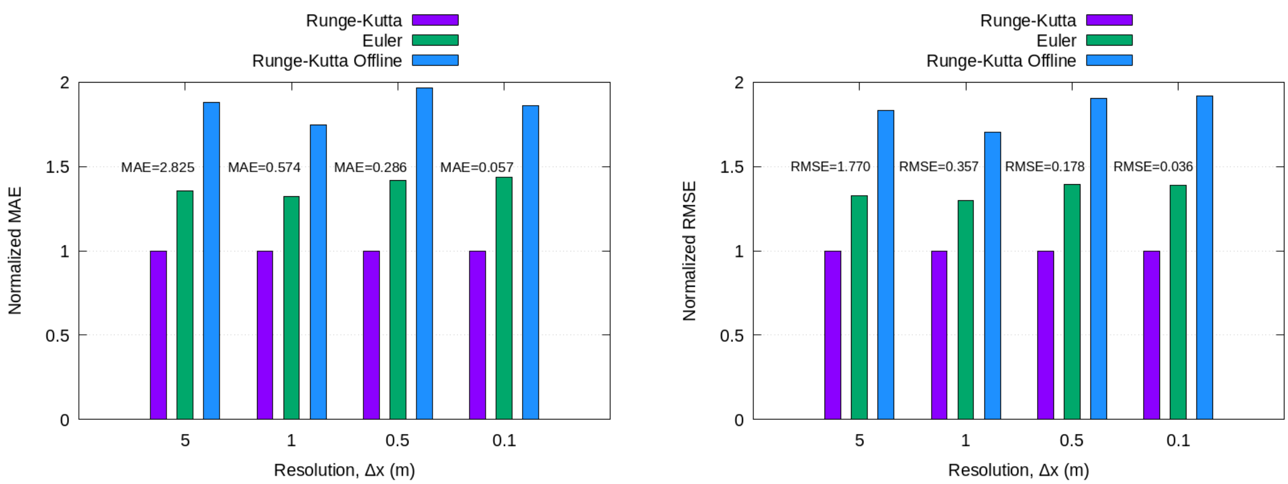

(a) (b)

Figure 6. Errors simulating the steady circular vortex case for the different numerical methods: normalized MAE **(a)** by the Euler error and normalized RMSE **(b)** by the Euler error.

4.2 Transient test case

Following the accuracy assessment, an analysis of computational efficiency is conducted using a well-known test case (see Figure 7a). The details of the experimental setup are described in (Soares-Frazão and Zech, 2008), where the domain dimensions described are $L = 36$ m in length, $B = 3.6$ m in width. As the initial condition, an initial water depth of 0.4 m in the reservoir region and 0 m in the right region are imposed, modying the value of the initial condition in the right region compared to the original experiment to check the accuracy of the model when wet-dry situations occur. The comparative analysis is based on increasing the number of particles to evaluate the model computational cost for each configuration. Moreover, this case is used as a validation of the model's ability to correctly resolve wet-dry situations. Reflective boundary conditions are applied every-

https://doi.org/10.5194/egusphere-2025-722
Preprint. Discussion started: 15 April 2025

Table 1. Computational cost for different number of particles using the numerical methods implemented and the increase ratio between simulation with particles and without particles, for the dam break test case.

Numerical method	Number of particles	Computational cost (s)	Increase ratio
Euler	10000	13.15	1.08
Euler	100000	21.22	1.75
Euler	1000000	66.59	5.48
Runge-Kutta	10000	30.00	2.47
Runge-Kutta	100000	121.93	10.03
Runge-Kutta	1000000	1043.56	85.89
Runge-Kutta Offline $5\Delta t$	10000	18.89	1.55
Runge-Kutta Offline $5\Delta t$	100000	60.93	5.01
Runge-Kutta Offline $5\Delta t$	1000000	474.24	39.03

where, maintaining a constant number of particles throughout the simulation. The Runge-Kutta offline method was updated using different time periods ($5\Delta t$, $10\Delta t$, $20\Delta t$ and $50\Delta t$, where Δt is the hydrodynamic time step) to analyze the influence of this variable in the temporal evolution of the particles position.

The computational costs for the different configurations with different particle numbers are shown in Table 1, where only the Runge-Kutta offline computational costs updated every 5 time steps are shown because it is the less computationally efficient case for the simulated Runge-Kutta offline combinations. The computational time for this simulation without particles was 12.15 seconds, and an overhead ratio relative to the hydrodynamic-only run is computed for each case. The forward Euler method consistently demonstrated shorter computational times compared to other methods across all configurations. Additionally, four states during the simulation are depicted in Figure 7, illustrating realistic particle trajectories simulated with the Euler scheme without traversing dry cells or climbing over buildings. However, when the Runge-Kutta offline is updated using long time periods, the temporal evolution of particles position can be illogical, as shown in Figure 8, where it can be seen some particles climbing over buildings. Finally, the differences between the methods' results are shown in Figure 9, where the L_2-norm per particle is derived from the differences between models, taking the Runge Kutta online method as the basis for comparison. The error between the Euler and Runge-Kutta methods is lower than the errors between the Runge-Kutta and Runge-Kutta offline methods, indicating that the Euler method provides results more similar to the Runge-Kutta method while maintaining higher computational efficiency. In addition, as the update time for the offline Runge-Kutta method increases, the difference between the online Runge-Kutta and the offline Runge-Kutta increases too, due to the fact that being a transient case, not updating frequently can lead to a high error.

https://doi.org/10.5194/egusphere-2025-722
Preprint. Discussion started: 15 April 2025

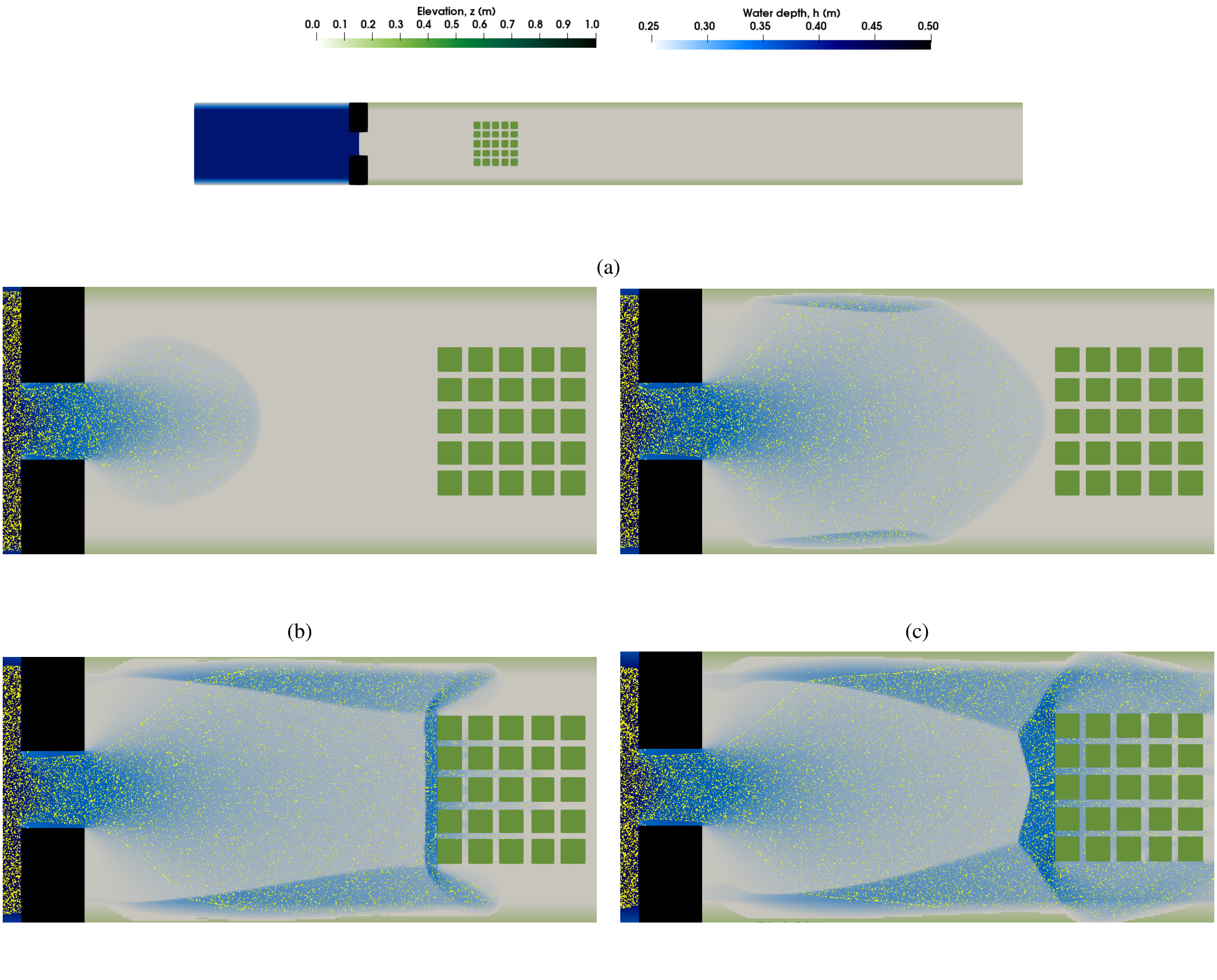

Figure 7. Initial condition of the transient test case (a). States at $t = 5s$ (**b**), at $t = 10s$ (**c**), at $t = 15s$ (**d**), and at $t = 20s$ (**e**) for the Euler method with 100000 particles in the dam break case.

4.3 Channel with cavities

A longitudinal channel with symmetrically shaped cavities was simulated, using a mesh with a resolution of 2x2 cm (see Figure 10a). The objective is to check whether a symmetrical distribution of particles is achieved across the upper and lower cavities (Vallés et al., 2023). 1000000 particles were simulated with an initial distribution as shown in Figure 10a. Given the

https://doi.org/10.5194/egusphere-2025-722
Preprint. Discussion started: 15 April 2025

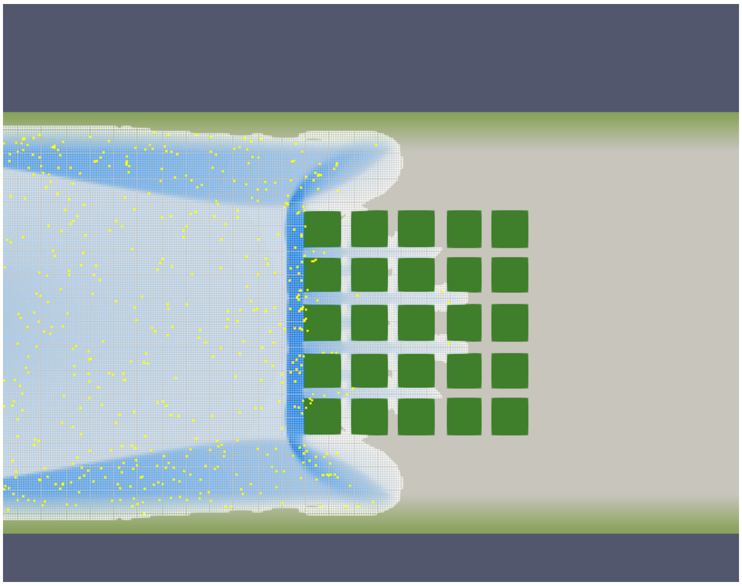

Figure 8. State with particles climbing over buildings for the Runge-Kutta offline $50\Delta t$.

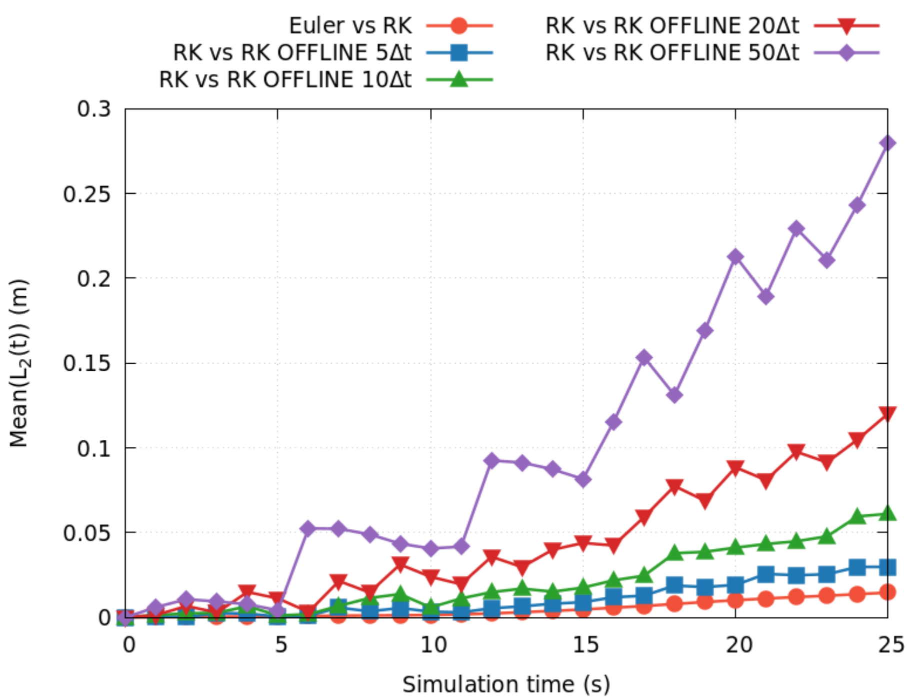

Figure 9. Temporal evolution of the L_2-norm per particle obtained from the difference between methods results.

https://doi.org/10.5194/egusphere-2025-722
Preprint. Discussion started: 15 April 2025

310 best compromise between accuracy and computational efficiency in the last test cases, the Euler method was only employed for this simulation. The temporal evolution of the particles position with and without turbulence was compared (see Figure 10), with the evolution of particle numbers in each pair of upper and lower cavities depicted in Figure 11. The presence of turbulence resulted in greater dispersion in particle distribution and more realistic trajectories compared to simulations without turbulence. This is further evidenced in Figure 11, where the number of particles within a cavity is higher when turbulence is
315 considered. The symmetry between the upper and lower cavities (see Figure 11), regardless of whether turbulence is added or not, provides a further argument for the accuracy of the Lagrangian model.

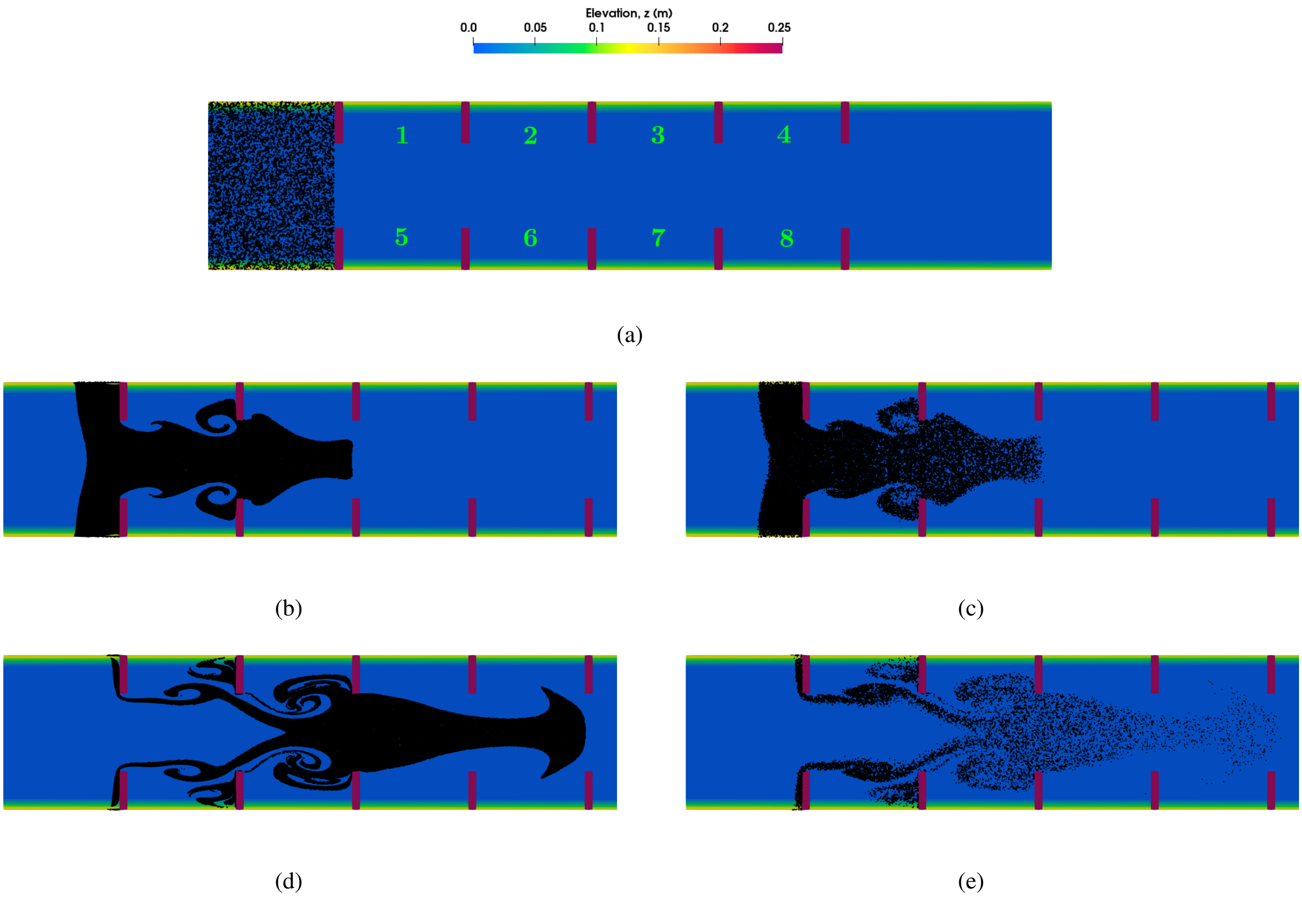

Figure 10. Initial condition for the cavities test case with 10000 particles with the numeration of the polygons (a). States with zoom at $t = 50s$ without turbulence (b) and with turbulence (c), and at $t = 100s$ without turbulence (d) and with turbulence (e).

https://doi.org/10.5194/egusphere-2025-722
Preprint. Discussion started: 15 April 2025

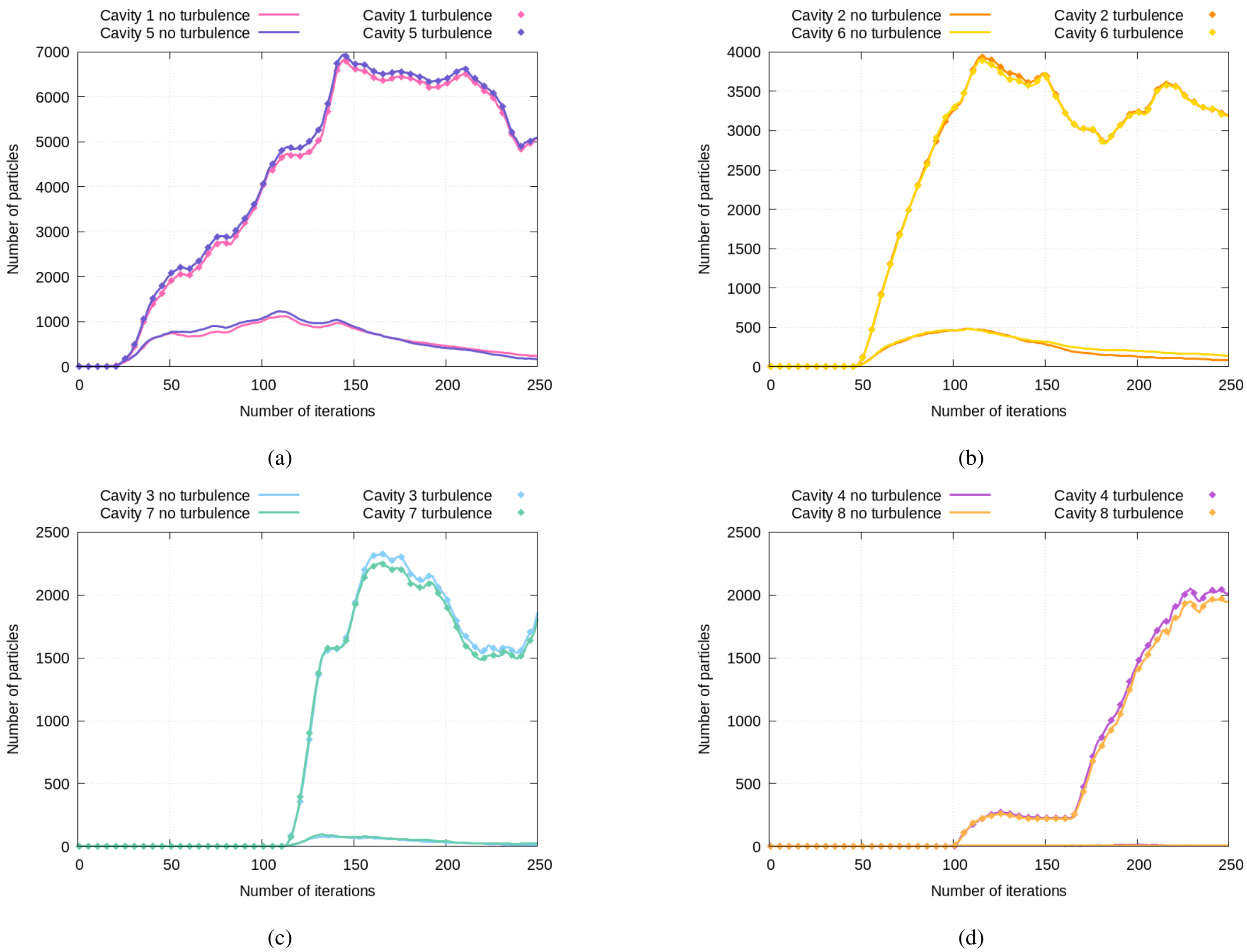

Figure 11. Number of particles inside of the different cavities (cavities 1 and 5 in Figure **(a)**, cavities 2 and 6 in Figure **(b)**, cavities 3 and 7 in Figure **(c)**, and cavities 4 and 8 in Figure **(d)**) for each iteration.

4.4 Example application: surface runoff in the Arnás catchment

The implemented Lagrangian model may have applications in ecohydrology, such as seed, pollutant, or nutrient transport. Consequently, a case involving a precipitation event over the Arnás catchment was simulated to show the potential application of this model. This catchment is located in the Borau valley (Northern Spanish Pyrenees). In the last decades, this region has been an area of exhaustive study of different hydrological processes (Lana-Renault et al., 2007; García-Ruiz et al., 2005). Physical processes such as rainfall, infiltration, runoff generation, and gully formation have been simulated in detail using various methods (López-Barrera et al., 2011; Fernández-Pato et al., 2016; Vallés et al., 2024). The primary objective of simulating this case was to assess its potential utility in environmental applications. Information derived from conservative tracers and

https://doi.org/10.5194/egusphere-2025-722
Preprint. Discussion started: 15 April 2025

field experiments measuring isotopes in water has been widely used in hydrology to characterize hydrological pathways and connectivity, with ideas such as transit or residence times, and travel time distributions (Benettin et al., 2022). Here, we show a minimal example of how analogous ideas can be investigated within the computational modelling setting we propose.

The catchment was discretized at 5m resolution, for a total of 110000 computational cells. 10000 number of particles were randomly placed in the domain as initial condition for the Lagrangian model, and the catchment was initially dry for the shallow water solver.

Two real precipitation cases (see Figure 13) were simulated to analyze the particle trajectory behaviour under different hyetographs. The particles trajectories for the event 1 are shown for two states in Figure 14. As shown in these figure, particles are mostly transported through the main gullies.

Runtime for the simulations of the events 1 and 2 were 317.75s and 177.02s respectively, providing an overhead of 2.39 and 1.10 compared to the same simulations without the particles.

Additionally, the total travelled distance per particle, the particle travel time and the time during which the particle was stationary are shown in Figures 15, 16 and 17 for each precipitation event. These figures provide a statistical overview of particle dynamics during the runoff events. Physically, these metrics offer insights into the hydrological processes at play. The covered distance reflects the efficiency of the drainage network of the basin to transport the debris, which can be seen in Figure 15b, where most of the particles travel a distance very similar to the initial one with respect to the outlet boundary condition. Moreover, it is observed in Figure 15a that a set of particles of event 2 travels much more than the rest of particles. This is due to the properties of this precipitation event, being a less intense but longer event than event 1. This might cause travelling particles for larger times (and smaller stop times), as also observed in Figure 17b. Furthermore, this stationary time histogram reveals areas of stagnant transport, where particles are halted due to reduced flow velocities or topographical barriers, leading to storage areas, or potential sediment deposition areas. However, as shown in Figure 16, the set of particles with high covered distances does not influence the last hours of the temporal evolution of the total covered distance (see Figure 16) because in both events the majority of the particles go out the domain. However, the difference between the events are higher at the beginning of the case, having a big difference between both hyetographs in the first hours. In event 1, the higher frequency of particles compared to the event 2 with extended stationary times suggests intermittent flow conditions, possibly due to intermittent rainfall, leading to temporary particle deposition. In contrast, event 2 exhibits more uniform movement and shorter stationary times, likely due to less intermittent rainfall that fosters persistent particle transport. Thus, these histograms not only quantify particle behavior but also provide insights into the underlying hydrological and geomorphological processes shaping the catchment's response to precipitation events.

5 Conclusions

In this work, we presented a Lagrangian model for particle transport implemented within the SERGHEI framework. This model utilizes an algorithm that leverages information from each cell occupied by the particles and is solved using three methods: an online first order Euler method, an online fourth order Runge-Kutta method, and an offline fourth order Runge-Kutta method.

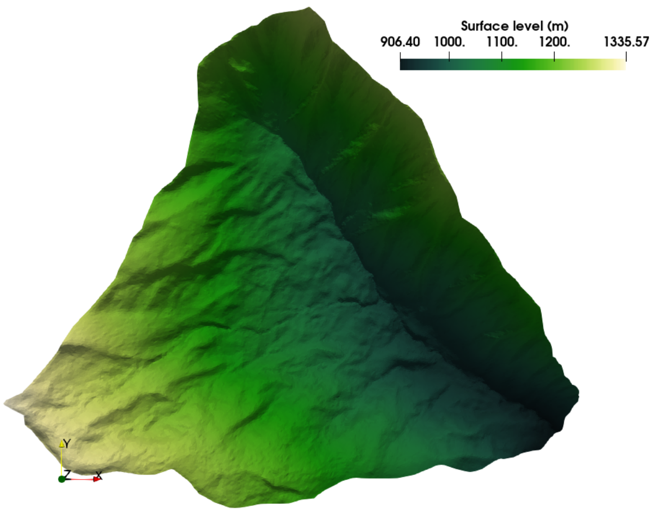

Figure 12. 3D representation of the Arnás catchment.

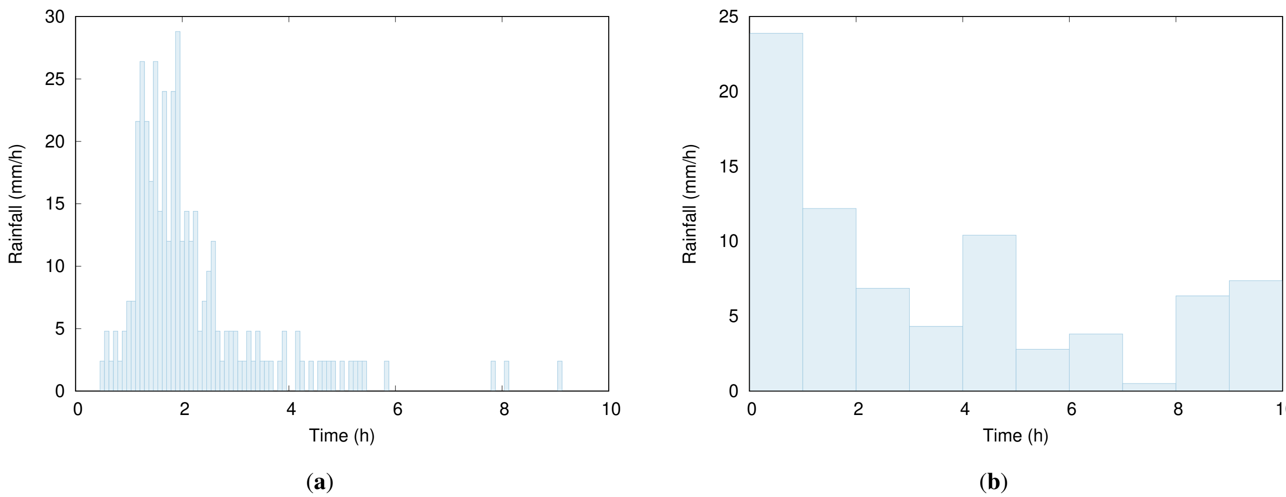

Figure 13. Hyetograph 1 **(a)** and hyetograph 2 **(b)** for the Arnás case.

We studied convergence and accuracy of the solvers with a steady circular vortex benchmark case. All methods yielded similar error metrics, with good grid convergence behaviour.

Subsequently, we conducted a transient test case without dispersive terms to assess the computational efficiency of the methods and to verify the accurate simulation of dry-wet conditions for the particles. The results indicate that the Euler method is the most efficient, with smaller differences in performance compared to the Runge-Kutta methods. Moreover, as shown in Figure 9, the Runge-Kutta offline method can result in incorrect trajectories because of the dry cells presence. Thus, we

https://doi.org/10.5194/egusphere-2025-722
Preprint. Discussion started: 15 April 2025

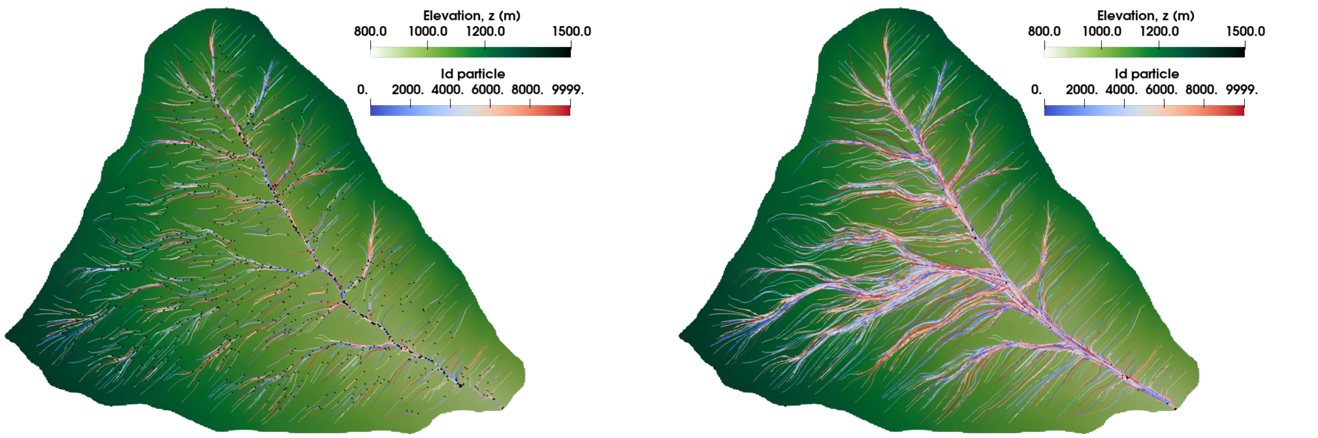

(a) (b)

Figure 14. States for the particles trajectories at the middle of precipitation event 1 **(a)** and at the end **(b)**.

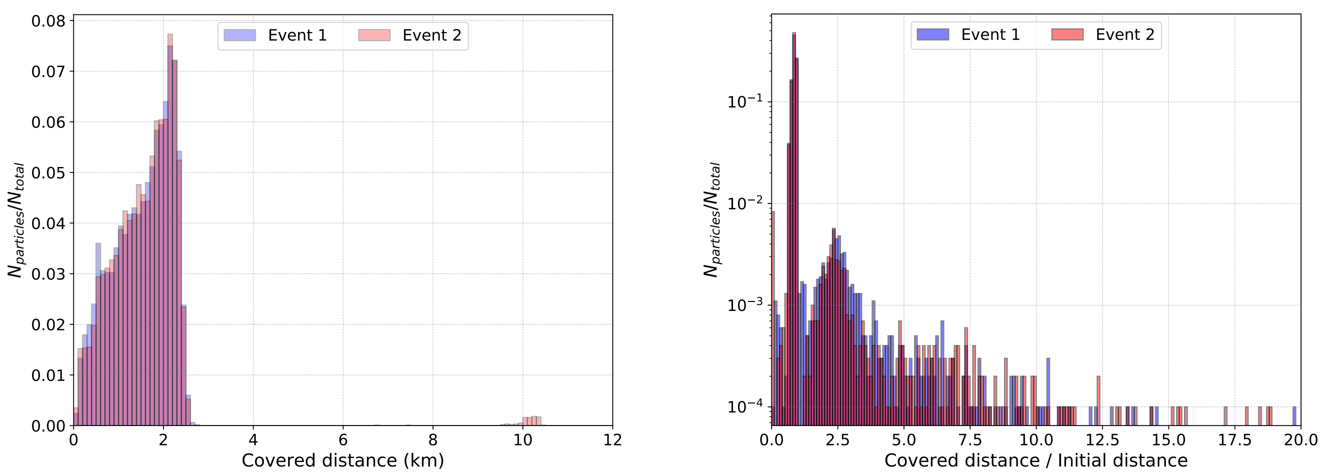

(a) (b)

Figure 15. Histograms of the covered distance **(a)** and the covered distance normalised by the initial distance between the particle and the boundary condition position for both precipitation events **(b)**.

conclude that the Euler method strikes the best balance between accuracy and computational efficiency, effectively addressing potential dry-wet issues. The high accuracy of the Euler method is obtained because the time step for the numerical scheme is sufficiently small.

To investigate the impact of turbulence, we simulated a channel with multiple cavities both with and without turbulence. The results illustrate that incorporating turbulence significantly alters particle trajectories, resulting in more realistic transport

https://doi.org/10.5194/egusphere-2025-722
Preprint. Discussion started: 15 April 2025

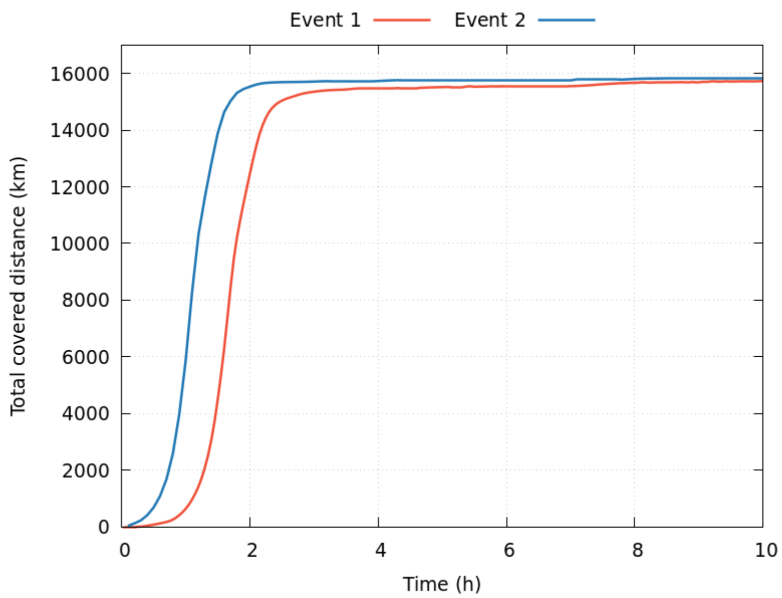

Figure 16. Temporal evolution of the total covered distance for both events.

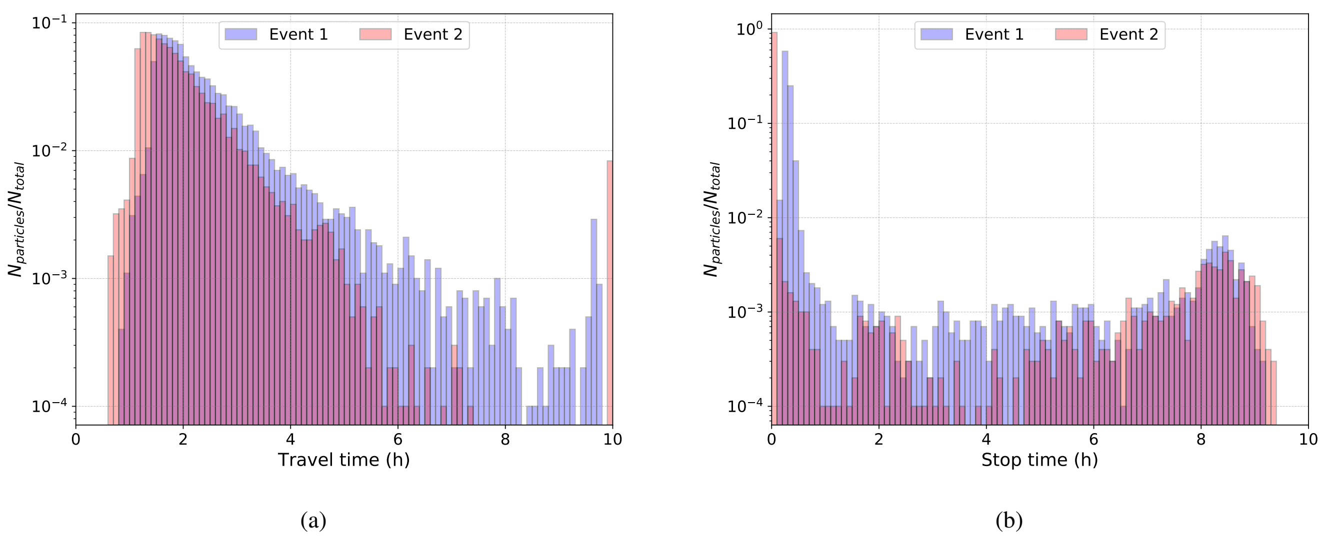

Figure 17. Histograms of the travel time **(a)** and the stop time **(b)**.

dynamics. However, as it is shown in previous work (Vallés et al., 2024), the addition of the turbulence implies a relevant
370 increasing of the computational cost.

Finally, the model was applied to a realistic case study of the Arnás catchment. The output generated by the model offers significant insights for environmental applications. The results elucidate the mechanisms of particle transport during precipita-

https://doi.org/10.5194/egusphere-2025-722
Preprint. Discussion started: 15 April 2025

tion events and identify the primary gullies that facilitate this transport. Furthermore, this information provides critical insights into the dynamics of particle movement, revealing distinct patterns in both movement and stationary times. These patterns reflect the influence of varying precipitation intensities and can help on identifying sediment mobilization and deposition processes within the catchment. This analysis underscores the potential of such models to enhance our understanding of different multiscale complex phenomena that take places in a catchment.

In summary, the Euler method delivers results comparable in accuracy to the other methods while offering superior computational efficiency. Furthermore, the Lagrangian model for particles transport effectively simulates realistic events by incorporating a minimal representation of turbulence, enhancing the realism of particle transport. Future work will focus on optimizing the model to further reduce computational costs and implementing multi-GPU simulations to leverage the capabilities of the SERGHEI hydrodynamic model.

Code and data availability. SERGHEI is available through GitLab, at https://gitlab.com/serghei-model/serghei, under a 3-clause BSD license. SERGHEI v2.1.0 was tagged as the first release of the LPT module at the time of submission of this paper. Static code for v2.1.0 can be found at https://doi.org/10.5281/zenodo.14871005 (Vallés et al., 2025b). This release does not include the Runge-Kutta solver. Static code for the experimental solution with Runge-Kutta integrators can be found at https://doi.org/10.5281/zenodo.14870918 (Vallés et al., 2025a). A repository containing test cases is available https://gitlab.com/serghei-model/serghei-tests/lpt.

Author contributions. PV: Investigation, Methodology, Software, Validation, Writing - Original Draft Preparation. DCV: Supervision, Conceptualization, Methodology, Software, Formal analysis, Data Curation, Writing - Review and Editing. MMH: Supervision, Funding acquisition, Conceptualization, Methodology, Formal analysis, Writing - Review and Editing. VR: Supervision, Funding acquisition, Writing - Review and Editing. PGN: Funding acquisition, Writing - Review and Editing.

Competing interests. No competing interests exist.

Acknowledgements. Pablo Vallés is funded by the UPPA-UNIZAR Research Grant PI-PRD/2022-03 and he was funded by ERASMUS+ KA103 "IBERUS+" 2021-1-ES01-KA130-HED-000004265. This work was partially funded by the project JIUZ2023-IA-04 by UNIZAR.

https://doi.org/10.5194/egusphere-2025-722
Preprint. Discussion started: 15 April 2025

References

Arcement, G. and Schneider, V.: Guide for Selecting Manning's Roughness Coefficients for Natural Channels and Flood Plains, no. 2339 in U.S. Geological Survey. Water-supply paper, 1984.

Baharvand, S., Ahmari, H., and Taghvaei, P.: Developing a Lagrangian sediment transport model for open channel flows, International Journal of Sediment Research, 38, 153–165, https://doi.org/https://doi.org/10.1016/j.ijsrc.2022.09.003, 2023.

Bates, P. D., Savage, J., Wing, O., Quinn, N., Sampson, C., Neal, J., and Smith, A.: A climate-conditioned catastrophe risk model for UK flooding, Natural Hazards and Earth System Sciences, 23, 891–908, https://doi.org/10.5194/nhess-23-891-2023, 2023.

Bayón, A., Valero, D., and Franca, M. J.: Urban flood drifters (UFD): Identification, classification and characterisation, Journal of Flood Risk Management, n/a, e13 002, https://doi.org/https://doi.org/10.1111/jfr3.13002, 2024.

Benettin, P., Rodriguez, N. B., Sprenger, M., Kim, M., Klaus, J., Harman, C. J., van der Velde, Y., Hrachowitz, M., Botter, G., McGuire, K. J., Kirchner, J. W., Rinaldo, A., and McDonnell, J. J.: Transit Time Estimation in Catchments: Recent Developments and Future Directions, Water Resources Research, 58, https://doi.org/10.1029/2022wr033096, 2022.

Bennett, J. R. and Clites, A. H.: Accuracy of trajectory calculation in a finite-difference circulation model, Journal of Computational Physics, 68, 272–282, https://doi.org/https://doi.org/10.1016/0021-9991(87)90058-1, 1987.

Braudrick, C. A. and Grant, G. E.: When do logs move in rivers?, Water Resources Research, 36, 571–583, https://doi.org/https://doi.org/10.1029/1999WR900290, 2000.

Cai, C., Zhu, L., and Hong, B.: A review of methods for modeling microplastic transport in the marine environments, Marine Pollution Bulletin, 193, 115 136, https://doi.org/https://doi.org/10.1016/j.marpolbul.2023.115136, 2023.

Caviedes-Voullième, D., Morales-Hernández, M., Norman, M. R., and Özgen-Xian, I.: SERGHEI (SERGHEI-SWE) v1.0: a performance-portable high-performance parallel-computing shallow-water solver for hydrology and environmental hydraulics, Geoscientific Model Development, 16, 977–1008, https://doi.org/10.5194/gmd-16-977-2023, 2023.

Chen, J., Hill, A. A., and Urbano, L. D.: A GIS-based model for urban flood inundation, Journal of Hydrology, 373, 184–192, 2009.

Cunge, J. A., Holly, F. M., and Verwey, A.: Practical aspects of computational river hydraulics, Pitman Pub. Inc, 1989.

De Cicco, P., Enio, P., and Solari, L.: Flume experiments on bridge clogging by woody debris: The effect of shape of piers, https://doi.org/10.13140/RG.2.1.4630.6648, 2015.

Dottori, F., Szewczyk, W., Ciscar, J.-C., Zhao, F., Alfieri, L., Hirabayashi, Y., Bianchi, A., Mongelli, I., Frieler, K., Betts, R. A., and Feyen, L.: Increased human and economic losses from river flooding with anthropogenic warming, Nature Climate Change, 8, 781–786, 2018.

Echeverribar, I., Morales-Hernández, M., Brufau, P., and García-Navarro, P.: 2D numerical simulation of unsteady flows for large scale floods prediction in real time, Advances in Water Resources, 134, 103 444, 2019.

Fernández-Pato, J., Caviedes-Voullième, D., and García-Navarro, P.: Rainfall/runoff simulation with 2D full shallow water equations: Sensitivity analysis and calibration of infiltration parameters, Journal of Hydrology, 536, 496–513, https://doi.org/https://doi.org/10.1016/j.jhydrol.2016.03.021, 2016.

Finaud-Guyot, P., Hétier, M., and Rousseau, A.: Numerical modeling of large debris transport during floods, working paper or preprint, 2023.

for Research on the Epidemiology of Disasters (CRED), C. and for Disaster Risk Reduction (UNDRR), U. O.: Human Cost of Disasters: An overview of the last 20 years (2000-2019), Centre for Research on the Epidemiology of Disasters (CRED), Brussels, 2020.

Formetta, G. and Feyen, L.: Empirical evidence of declining global vulnerability to climate-related hazards, Global Environmental Change, 57, 101 920, https://doi.org/https://doi.org/10.1016/j.gloenvcha.2019.05.004, 2019.

García-Martínez, R. and Flores-Tovar, H.: Computer Modeling of Oil Spill Trajectories With a High Accuracy Method, Spill Science & Technology Bulletin, 5, 323–330, https://doi.org/https://doi.org/10.1016/S1353-2561(99)00077-8, 1999.

García-Ruiz, J., Arnáez, J., Beguería, S., Seeger, M., Martí-Bono, C., Regüés, D., Lana-Renault, N., and White, S.: Runoff generation in an intensively disturbed, abandoned farmland catchment, Central Spanish Pyrenees, CATENA, 59, 79–92, https://doi.org/https://doi.org/10.1016/j.catena.2004.05.006, 2005.

Horn, S., Raabe, A., Will, H., and Tackenberg, O.: TurbSeed—A model for wind dispersal of seeds in turbulent currents based on publicly available climate data, Ecological Modelling, 237-238, 1–10, https://doi.org/https://doi.org/10.1016/j.ecolmodel.2012.04.009, 2012.

Ivshina, I., Kuyukina, M., Krivoruchko, A., Elkin, A., Makarov, S., Cunningham, C., Peshkur, T., Atlas, R., and Philp, J.: Oil spill problems and sustainable response strategies through new technologies, Environmental Science: Processes and Impacts, 17, 1201–1219, https://doi.org/10.1039/c5em00070j, 2015.

Jalón-Rojas, I., Wang, X., and Fredj, E.: A 3D Numerical Model to Track Marine Plastic Debris (TrackMPD): Sensitivity of Microplastic Trajectories and Fates to Particle Dynamical Properties and Physical Processes, Marine Pollution Bulletin, 141, 256–272, https://doi.org/10.1016/j.marpolbul.2019.02.052, 2019.

Knijff, J. M. V. D., Younis, J., and Roo, A. P. J. D.: LISFLOOD: A GIS-based distributed model for river basin scale water balance and flood simulation, International Journal of Geographical Information Science, 24, 189–212, 2010.

Lacasta, A., Morales-Hernández, M., Murillo, J., and García-Navarro, P.: An optimized GPU implementation of a 2D free surface simulation model on unstructured meshes, Advances in Engineering Software, 78, 1–15, 2014.

Lana-Renault, N., Latron, J., and Regüés, D.: Streamflow response and water-table dynamics in a sub-Mediterranean research catchment (Central Pyrenees), Journal of Hydrology, 347, 497–507, https://doi.org/https://doi.org/10.1016/j.jhydrol.2007.09.037, 2007.

Lebreton, L.-M., Greer, S., and Borrero, J.: Numerical modelling of floating debris in the world's oceans, Marine Pollution Bulletin, 64, 653–661, https://doi.org/https://doi.org/10.1016/j.marpolbul.2011.10.027, 2012.

Liubartseva, S., Coppini, G., Lecci, R., and Clementi, E.: Tracking plastics in the Mediterranean: 2D Lagrangian model, Marine Pollution Bulletin, 129, 151–162, https://doi.org/https://doi.org/10.1016/j.marpolbul.2018.02.019, 2018.

Lofty, J., Valero, D., Moreno-Rodenas, A., Belay, B. S., Wilson, C., Ouro, P., and Franca, M. J.: On the vertical structure of non-buoyant plastics in turbulent transport, Water Research, 254, 121 306, https://doi.org/https://doi.org/10.1016/j.watres.2024.121306, 2024.

López-Barrera, D., Navarro, P. G., and Brufau, P.: Sources of uncertainty in the validation of a coupled hydrological-hydraulic simulation model with sediment transport, La Houille Blanche, 97, 17–22, https://doi.org/10.1051/lhb/2011027, 2011.

Martin, J., Henrichs, T., Clark, B., Stanners, D., McInnes, G., McGlade, J., Petersen, J., Huntington, J., Vos, H., McAleavey, P., et al.: The European environment-state and outlook 2010: Synthesis, Publications Office of the European Union, 2010.

Martínez-Gomariz, E., Russo, B., Gómez, M., and Plumed, A.: An approach to the modelling of stability of waste containers during urban flooding, Journal of Flood Risk Management, 13, e12 558, https://doi.org/https://doi.org/10.1111/jfr3.12558, 2020.

Mellink, Y. A. M., van Emmerik, T. H. M., and Mani, T.: Wind- and rain-driven macroplastic mobilization and transport on land, Scientific Reports, 14, 3898, 2024.

Merritt, D. M. and Wohl, E. E.: Processes governing hydrochory along rivers: Hydraulics, hydrology, and dispersal phenology, Ecological Applications, 12, 1071–1087, https://doi.org/https://doi.org/10.1890/1051-0761(2002)012[1071:PGHARH]2.0.CO;2, 2002.

Molazadeh, M., Calabro, G., Liu, F., Tassin, B., Rovelli, L., Lorke, A., Dris, R., and Vollertsen, J.: The role of turbulence in the deposition of intrinsically buoyant MPs, Science of The Total Environment, 911, 168 540, https://doi.org/https://doi.org/10.1016/j.scitotenv.2023.168540, 2024.

https://doi.org/10.5194/egusphere-2025-722
Preprint. Discussion started: 15 April 2025

Morales-Hernández, M., García-Navarro, P., Burguete, J., and Brufau, P.: A conservative strategy to couple 1D and 2D models for shallow water flow simulation, Computers & Fluids, 81, 26 – 44, 2013.

Morales-Hernández, M., Murillo, J., and García-Navarro, P.: Diffusion-dispersion numerical discretization for solute transport in 2D transient shallow-flows, Environmental Fluid Mechanics, 9, 1217–1234, 2019.

Morales-Hernández, M., Sharif, M. B., Kalyanapu, A., Ghafoor, S., Dullo, T., Gangrade, S., Kao, S.-C., Norman, M., and Evans, K.: TRITON: A Multi-GPU open source 2D hydrodynamic flood model, Environmental Modelling & Software, 141, 105 034, https://doi.org/https://doi.org/10.1016/j.envsoft.2021.105034, 2021.

Murillo, J. and García-Navarro, P.: Weak solutions for partial differential equations with source terms: Application to the shallow water equations, Journal of Computational Physics, 229, 4237–4368, 2010.

Nations, U.: Sendai Framework for Disaster Risk Reduction 2015-2030, United Nations, 2015.

Nordam, T., Kristiansen, R., Nepstad, R., van Sebille, E., and Booth, A. M.: A comparison of Eulerian and Lagrangian methods for vertical particle transport in the water column, Geoscientific Model Development, 16, 5339–5363, https://doi.org/10.5194/gmd-16-5339-2023, 2023.

OECD: Financial Management of Flood Risk, OECD Publishing, Paris, https://doi.org/https://doi.org/10.1787/9789264257689-en, 2016.

Olcina, J., Sauri, D., Hernández, M., and Ribas, A.: Flood policy in Spain: a review for the period 1983-2013, Disaster Prevention and Management, 25, 41–58, 2016.

Peeters, F. and Hofmann, H.: Length-Scale Dependence of Horizontal Dispersion in the Surface Water of Lakes, Limnology and Oceanography, 60, 1917–1934, 2015.

Persi, E., Petaccia, G., and Sibilla, S.: Large wood transport modelling by a coupled Eulerian–Lagrangian approach, Natural Hazards, 91, 59–74, iD: Persi2018, 2018a.

Persi, E., Petaccia, G., Sibilla, S., Brufau, P., and García-Navarro, P.: Calibration of a dynamic Eulerian-lagrangian model for the computation of wood cylinders transport in shallow water flow, Journal of Hydroinformatics, 21, 164–179, https://doi.org/10.2166/hydro.2018.085, 2018b.

Pilechi, A., Mohammadian, A., and Murphy, E.: A numerical framework for modeling fate and transport of microplastics in inland and coastal waters, Marine Pollution Bulletin, 184, 114 119, https://doi.org/https://doi.org/10.1016/j.marpolbul.2022.114119, 2022.

Portillo De Arbeloa, N. and Marzadri, A.: Modeling the transport of microplastics along river networks, Science of The Total Environment, 911, 168 227, https://doi.org/https://doi.org/10.1016/j.scitotenv.2023.168227, 2024.

Ripple, W. J., Wolf, C., Newsome, T. M., Barnard, P., and Moomaw, W. R.: World scientists' warning of a climate emergency, BioScience, 70, 8–100, 2020.

Rutherford, J.: River Mixing, Wiley, Chichester, 1994.

Sampson, C. C., Smith, A. M., Bates, P. D., Neal, J. C., Alfieri, L., and Freer, J. E.: A high-resolution global flood hazard model, Water Resources Research, 51, 7358–7381, https://doi.org/https://doi.org/10.1002/2015WR016954, 2015.

Schreyers, L. J., van Emmerik, T. H., Huthoff, F., Collas, F. P., Wegman, C., Vriend, P., Boon, A., de Winter, W., Oswald, S. B., Schoor, M. M., Wallerstein, N., van der Ploeg, M., and Uijlenhoet, R.: River plastic transport and storage budget, Water Research, p. 121786, https://doi.org/https://doi.org/10.1016/j.watres.2024.121786, 2024.

Soares-Frazão, S. and Zech, Y.: Dam-break flow through an idealised city, Journal of Hydraulic Research, 46, 648–658, https://doi.org/10.3826/jhr.2008.3164, 2008.

Sánchez-Salas, J., Flores, J., Jurado, E., Sáenz-Mata, J., Orozco-Figueroa, P., and Muro Pérez, G.: Hidrocoria en semillas de Agave victoriae-reginae T. Moore, especie en peligro de extinción: Morfología y anatomía como facilitadores de la hidro-dispersión y germinación, Gayana. Botánica, 74, 251–261, https://doi.org/10.4067/S0717-66432017000200251, 2017.

Thielen, J., Bartholmes, J., Ramos, M.-H., and De Roo, A.: The European flood alert system–part 1: concept and development, Hydrology and Earth System Sciences, 13, 125–140, 2009.

Thomas, H. and Nisbet, T.: Modelling the hydraulic impact of reintroducing large woody debris into watercourses, Journal of Flood Risk Management, 5, 164–174, https://doi.org/https://doi.org/10.1111/j.1753-318X.2012.01137.x, 2012.

Vacondio, R., Aureli, F., Ferrari, F., Mignosa, P., and Dal Palù, A.: Simulation of the January 2014 flood on the Secchia River using a fast and high-resolution 2D parallel shallow-water numerical scheme, Natural Hazards, 80, 103 – 125, 2016.

Valero, D., Bayón, A., and Franca, M. J.: Urban Flood Drifters (UFDs): Onset of movement, Science of The Total Environment, 927, 171 568, https://doi.org/https://doi.org/10.1016/j.scitotenv.2024.171568, 2024.

Vallés, P., Morales-Hernández, M., García-Navarro, P., Roeber, V., and Caviedes-Voullième, D.: Enhancing Flood Analysis with a Lagrangian Transport Modeling and SERGHEI, in: Advances in Hydroinformatics—SimHydro 2023 Volume 1, pp. 387–405, Springer, https://doi.org/10.1007/978-981-97-4072-7, 2023.

Vallés, P., Fernández-Pato, J., Morales-Hernández, M., Echeverribar, I., and García-Navarro, P.: A 2D shallow water flow model with 1D internal boundary condition for subgrid-scale topography, Advances in Water Resources, 189, 104 716, https://doi.org/https://doi.org/10.1016/j.advwatres.2024.104716, 2024.

Vallés, P., Caviedes-Voullième, D., and Morales-Hernández, M.: SERGHEI-LPT-RK, https://doi.org/10.5281/zenodo.14870918, 2025a.

Vallés, P., Caviedes-Voullième, D., and Morales-Hernández, M.: SERGHEI v2.1.0, https://doi.org/10.5281/zenodo.14871005, 2025b.

van Emmerik, T., Mellink, Y., Hauk, R., Waldschlaeger, K., and Schreyers, L.: Rivers as Plastic Reservoirs, Frontiers in Water, 3, 786 936, https://doi.org/10.3389/frwa.2021.786936, 2022.

Wallemacq, P., Guha-Sapir, D., McClean, D., CRED, and UNISDR: The Human Cost of Weather-Related Disasters 1995-2015, Centre for Research on the Epidemiology of Disasters (CRED), Brussels, 2015.

Xia, J., Teo, F. Y., Lin, B., and Falconer, R. A.: Formula of incipient velocity for flooded vehicles, Natural Hazards, 58, 1–14, 2011.

Xia, X., Liang, Q., and Ming, X.: A full-scale fluvial flood modelling framework based on a high-performance integrated hydrodynamic modelling system (HiPIMS), Advances in Water Resources, https://doi.org/10.1016/j.advwatres.2019.103392, 2019.

Yang, H. and Foroutan, H.: Effects of near-bed turbulence on microplastics fate and transport in streams, Science of The Total Environment, 905, 167 173, https://doi.org/https://doi.org/10.1016/j.scitotenv.2023.167173, 2023.

Zamora, C. O. and Montagnini, F.: Seed Rain and Seed Dispersal Agents in Pure and Mixed Plantations of Native Trees and Abandoned Pastures at La Selva Biological Station, Costa Rica, Restoration Ecology, 15, 453–461, https://doi.org/https://doi.org/10.1111/j.1526-100X.2007.00241.x, 2007.

Zhao, C., Fang, H., Ouro, P., Stoesser, T., and Dey, S.: Response of Bedload and Bedforms to Near-Bed Flow Structures, Journal of Hydraulic Engineering, 150, 04023 060, https://doi.org/10.1061/JHEND8.HYENG-13618, 2024.